Applied Catalysis B: Environmental 160–161 (2014) 558–565

Contents lists available at ScienceDirect

Applied Catalysis B: Environmental

journal homepage: www.elsevier.com/locate/apcatb

Synthesis of N-doped TiO_2 photocatalyst for low-concentration elemental mercury removal under various gas conditions

Shiao-Shing Chen[a], Hsing-Cheng Hsi[b,*], Sheng-Hung Nian[a], Chun-Hsiang Chiu[a]

[a] Institute of Environmental Engineering and Management, National Taipei University of Technology, No. 1, Sec. 3, Chung-Hsiao E. Rd., Taipei 106, Taiwan
[b] Graduate Institute of Environmental Engineering, National Taiwan University, Taipei, Taiwan, No. 71 Chou-Shan Rd., Taipei 106, Taiwan

ARTICLE INFO

Article history:
Received 31 October 2013
Received in revised form 7 March 2014
Accepted 8 May 2014
Available online 13 June 2014

Keywords:
Titanium dioxide
Nitrogen doping
Visible light
Elemental mercury
Flue gas component

ABSTRACT

This study proposes preparing N-doped TiO_2 nanoparticles that exhibit a narrow bandgap by calcinating a mixture of Degussa P-25 TiO_2 and NH_4Cl at a temperature of 400 °C under airtight conditions to remove gaseous elemental mercury (Hg^0). Sample characterization performed using X-ray photoelectron spectroscopy and ultraviolet-visible spectra indicated that the presence of Ti^{3+} caused by oxygen vacancy and molecular-state N may be incorporated into a TiO_2 lattice; this result was supported by an observation of the Ti–N group conducted using Fourier transform infrared spectroscopy. The formed nanoparticles exhibited a size of 32.4 nm and were in a mixed form of anatase and rutile according to the X-ray diffraction spectra. The low Hg removal of TiO_2 nanoparticles under the 0% O_2 dark condition indicated that photocatalytic oxidation limited Hg adsorption. The reemission of adsorbed Hg caused by H_2O competition for active sites can be markedly inhibited by N modification, which may be caused by strong bonding between Hg, N, and O groups. In addition, TiO_xN_y underwent less adsorption competition from humidity at an elevated temperature than an untreated sample did. NO exhibited substantial competition for the adsorption sites on the TiO_2 surface. By contrast, under dark conditions, both SO_2 and HCl slightly enhanced Hg adsorption; under ultraviolet and visible-light irradiation, both SO_2 and HCl markedly reduced Hg removal. SO_2 and HCl may substantially consume O_2^- and •OH free radicals during light irradiation and subsequently reduce the transformation of Hg^0 into HgO.

1. Introduction

Mercury (Hg) released from natural and anthropogenic sources has been a considerable global concern because it is toxic and bioaccumulative through the food chain [1]. The Minamata Convention on Mercury provided a substantial boost to the international effort to control Hg by convincing governments to agree to a global, legally binding treaty for preventing Hg emission and release [2]. Consequently, various large industrial facilities such as coal-fired utility boilers, industrial boilers, cement factories, smelters, and waste incinerators will be regulated to reduce Hg emissions. Typically, Hg can appear in three principal forms in combustion flue gas streams: elemental Hg (Hg^0), oxidized Hg (Hg^{2+}), and particle-bound Hg [3]. Hg^0 is highly volatile, insoluble in water, and, thus, difficult to capture using conventional air pollution control devices, such as wet flue gas desulfurization and electrostatic precipitators. Consequently, studies on enhancing Hg^0 adsorption and catalytic oxidation by using novel materials have been conducted extensively in recent years.

Titanium dioxide (TiO_2) has been observed to remove Hg^0 from the gas phase effectively through adsorption and catalytic oxidation [4–12]. Pitoniak et al. [4] removed gaseous Hg by using nanostructured SiO_2-TiO_2 composites. The samples containing 13% TiO_2 exhibited the greatest Hg removal. In addition, Pitoniak et al. [5] reported that Hg was adsorbed as both Hg^0 and Hg^{2+} onto an SiO_2-TiO_2 composite. Wu et al. [6] and Lee et al. [7] have selected in-situ generated titania particles irradiated using ultraviolet (UV) light to remove Hg from combustor exhaust. During irradiation by UV light, active sites were generated on a titania particle surface to adsorb Hg and form a complex ($TiO_2 \cdot HgO_{(complex)}$) on TiO_2. The Hg-containing TiO_2 nanoparticles were readily removed when the gas streams passed through conventional particle control devices [6].

Although removing Hg by using TiO_2 photocatalysis has been investigated extensively, the large bandgap energy of 3.2 eV enables only pure TiO_2 to be excited by UV light ($\lambda < 365$ nm) irradiation, limiting the application of TiO_2 photocatalysts. Because the solar energy utilization efficiency of TiO_2 is considerably low (only 3–4%), studies have been conducted to change the absorption edge of

* Corresponding author. Tel.: +886 2 33664374; fax: +886 2 23928830.
E-mail address: hchsi@ntu.edu.tw (H.-C. Hsi).

http://dx.doi.org/10.1016/j.apcatb.2014.05.022
0926-3373/

TiO_2 from a UV-light to visible-light (VL) region. Anionic nonmetal dopants, such as carbon [13], nitrogen [14,15], and sulfur [16], have been reported to exhibit a red-shifted absorption edge and to extend the photocatalytic activity into the visible light region for TiO_2. Despite several potential applications, N is the most effective material to substitute oxygen among the aforementioned anionic nonmetal dopants because its p state contributes to bandgap narrowing with O 2p states [14,15,17–19]. For example, Asahi et al. [14] prepared a N-doped TiO_2 film (TiO_xN_y) with an absorption threshold at 500 nm by using a sputtering method to decompose a methylene blue solution. In addition, Sato [17] reported that calcinating mixtures of $Ti(OH)_4$ and ammonium salts produced TiO_2-based materials that can be activated by VL irradiation. Additional reports have indicated that N-doped TiO_2 powders and films yield substantial improvements in VL absorption compared with pure TiO_2 [18,19].

Several approaches have been used for N doping, such as sputtering TiO_2 in an N_2-Ar atmosphere [20], heating TiO_2 or titanium hydroxide with N-containing organic compounds (e.g., urea, guanidine hydrochloride, and guanidine carbonate) [21] or in a NH_3 flow [22], and calcinating the hydrolysis product of a titanium precursor with ammonia [23]. However, multistep fabrication processes, including sample synthesis, calcination, and subsequent reduction, were required and few studies have focused on producing TiO_xN_y nanoparticles by using a single-step approach. Because no study has examined the photocatalytic effects of using N-containing TiO_2 under both UV and VL conditions at various temperatures on Hg^0 removal, this study involved preparing and characterizing TiO_xN_y nanoparticles from a mixture of Degussa P-25 TiO_2 and NH_4Cl by using a simple calcination method under airtight conditions and subsequently evaluating Hg^0 capture performance. The Hg^0 removal effectiveness of raw P-25 and TiO_xN_y in the presence of O_2, H_2O, and UV/VL irradiation was examined, and the influences of acidic flue gas components, namely SO_2, NO, and HCl, on Hg^0 removal were evaluated. The obtained results provided insight into the feasibility of applying surface-modified TiO_2 to remove low-concentration Hg^0 from flue gas steams and are crucial for developing innovative multipollutant control approaches.

2. Experimental

2.1. Preparation of TiO_xN_y nanoparticles

The TiO_xN_y powders used in this study were prepared using an airtight quartz tube inserted in a temperature-variable oven according to a method used in our previous research [24]. Commercial Degussa P-25 TiO_2 powder (P-25; approximately 80% anatase and 20% rutile with a surface area of 50 m^2/g) was thoroughly mixed with NH_4Cl powder and transferred to the airtight quartz tube. The calcined TiO_xN_y powders were prepared by heating the sample in air at 400 °C for 3 h, followed by continual calcination at 350 °C for 1 h. After the powders were air-cooled to room temperature, TiO_xN_y was obtained. The chemistry of these processes can be described by the succession of two reactions:

$$NH_4Cl \rightarrow NH_{3(g)} + HCl_{(g)} \quad (1)$$

$$TiO_2 + NH_{3(g)} + HCl_{(g)} \rightarrow TiO_xN_y + NH_4Cl_{(g)} + NO_{x(g)} \quad (2)$$

2.2. TiO_xN_y nanoparticle characterization

The microstructural properties of the raw and prepared N-doped TiO_2 samples were characterized using transmission electron microscopy (TEM; Hitachi, H-7100). The bandgap was measured by employing an ultraviolet-visible (UV/Vis) spectrometer technique using Cary 300 Bio equipped with an integrating sphere accessory for diffuse reflectance spectra. The chemical composition and valance state of Ti of the samples were verified using an X-ray photoelectron spectroscope (XPS; VG Scientific ESCALAB 250). Crystal structures were analyzed using X-ray diffraction (XRD; DMAX 2200 VK; Rigaku Co.). All of the peaks measured using XRD analysis were assigned by comparing them with those reported by the Joint Committee on Powder Diffraction Standards. Infrared spectra were measured using Fourier transform infrared spectroscopy (FTIR; Excalibur Series FTS-3500; Bio-Rad Laboratories Inc.). The Brunauer, Emmett, and Teller (BET) surface area was obtained from N adsorption–desorption data (Micromeritics, ASAP-2010). An assumption of spherical particles was used to convert the BET-specific surface areas into particle diameters.

2.3. Hg removal experiments

Raw P-25 and the synthesized TiO_xN_y were tested to evaluate the removal effectiveness of low-concentration Hg^0. The experimental apparatus, similar to that used in our previous study [10], comprised three major components: a mixing gas generation portion, photochemical reactor, and data acquisition system (Fig. 1). Hg^0 was generated using a certified Hg^0 permeation tube (VICI Metronics) at 70 ± 0.1 °C to ensure a constant Hg^0 diffusion rate. The generated Hg^0 with a known concentration was then mixed with O_2, N_2, and water vapor generated by flowing N_2 through a water bubbler. Both gas mixing and Hg^0 injection were conducted in a temperature-controlled chamber and heated tubes and lines to prevent water condensation. The generated Hg^0-containing gas at a concentration of 10–15 μg Hg^0 $N\,m^{-3}$ flowed at a rate of 1.5 $L\,min^{-1}$ through the photochemical reactor with 15 mg of TiO_2 homogeneously distributed onto six pieces of glass and irradiated with UV or VL. The UV lamp (F10T8BLB, Sankyo Denki) exhibits a wavelength within a range of 325–400 nm and a sharp peak at 364.5 nm. The VL lamp (ESS-DE-500 W, Philips) is a household halogen lamp exhibiting a broad peak between approximately 450 and 800 nm. Spectra of both light sources were obtained using a spectrophotometer (Ocean Optics, USB2000). Two UV lamps were used and placed approximately 5 cm from the photochemical reactor. The UV intensity (Lutron YK35-UV light meter) was 3.5 ± 0.5 mW cm^{-2}. Because of the strong light irradiation emitted from the VL lamp, the distance between the VL source and photochemical reactor was approximately 40 cm to control the measured intensity at 3.8–4.5 mW cm^{-2} (Lutron LX-103 light meter). UV light emitted from the VL lamp was weak; the intensity of this light at the reactor was approximately 0.01–0.03 mW cm^{-2}. To prevent interference, a thin polycarbonate plate was placed in front of the VL lamp to completely filter UV light.

The Hg^0 removal tests were performed at atmospheric pressure and at 25, 50, and 100 °C. In addition, the effects of acidic flue gas components, namely SO_2 (200 ppm_v), NO (200 ppm_v), and HCl (50 ppm_v), on Hg^0 removal were evaluated by individually introducing the gas component into the system at 6% O_2 with the presence of H_2O. Effluent gas from the photochemical reactor flowed through an impinger containing 10% $SnCl_{2(aq)}$, which reduced any oxidized Hg compounds to Hg^0. A moisture trap (i.e., a nefion tube) was installed downstream of the impinger to remove H_2O from the gas stream and prevent interference in Hg detection. The gas then flowed through a gold amalgamation column supported by a heating coil (Brooks Rand Lab model AC-01) where the Hg^0 in the gas was adsorbed. The Hg^0 that was concentrated on the gold was then thermally desorbed and sent as a concentrated Hg stream to a cold-vapor atomic fluorescence spectrophotometer (Brooks Rand Lab Model III) for analysis. Finally, the exhaust was passed through a carbon trap before being released into a fume

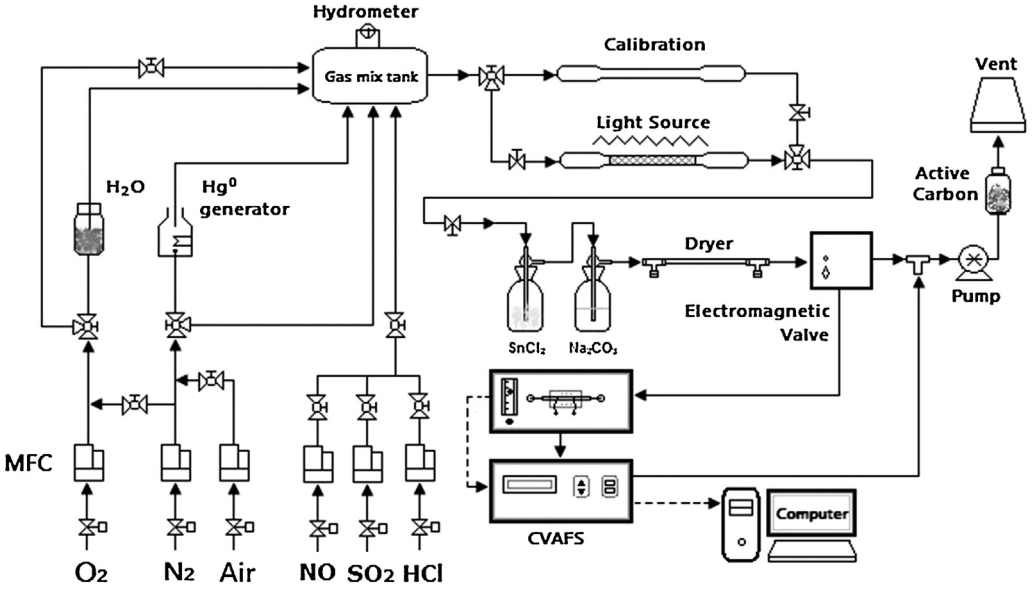

Fig. 1. Experimental apparatus for testing Hg^0 adsorption breakthrough.

hood. Each test run was completed in 6 min, and 10 runs were performed for each test condition. The average Hg^0 removal efficiency (E_{cap}) was calculated as follows:

$$E_{cap}(\%) = \frac{1}{n}\sum \frac{Hg^0_{in} - Hg_{T,out}}{Hg^0_{in}} \times 100 \quad (3)$$

where Hg^0_{in} denotes the inlet Hg^0 concentration; $Hg_{T,out}$ represents the outlet Hg concentration, including the original Hg^0 and the Hg^0 reduced from the photocatalytic Hg^{2+}; and $n = 10$ is the total test runs for a given condition. The blank experiments in which TiO_2 samples were not loaded in the reactor revealed negligible Hg^0 removal under all conditions.

3. Results and discussion

3.1. Characterization of TiO_xN_y nanoparticles

The prepared TiO_xN_y samples appeared to be yellowish white according to visual inspection. The TiO_xN_y catalysts characterized using XPS, UV/Vis absorption spectroscopy, FTIR, XRD, TEM, and BET-specific surface areas are discussed as follows. Fig. 2(a) shows a typical XPS survey spectrum of the TiO_xN_y sample. Ti $2p_{1/2}$, Ti $2p_{3/2}$, O 1s, and N 1s exhibited binding energies of 463.5, 457.8, 529.0, and 400.0 eV, respectively. The low intensity of the N peak is due to the lower sensitivity factor of N compared with those of Ti and O. The photoelectron signal of N at 400 eV indicated that N bound to O with a calculated doped N amount of 19.22 at.%. Because Ti–N bonding corresponding to the presence of TiN was not observed using XPS (i.e., Ti 2p = 455.8 eV and N 1s = 396.9 eV), N could be located in an interstitial site. Diwald et al. [25] observed that the N state (N 1s = 399.6 eV) introduced by NH_3 causes a shift of the photochemical threshold of TiO2, and this form of N is most likely located in an interstitial site bound to hydrogen. To elucidate the results, the Ti 2p spectra of the TiO_xN_y sample (Fig. 2(b)) were deconvoluted into four peaks within 456.4–464.4 eV; specifically Ti^{4+} $2p_{1/2}$, Ti^{3+} $2p_{1/2}$, Ti^{4+} $2p_{3/2}$, and Ti^{3+} $2p_{3/2}$ exhibited peaks at 464.6, 463.5, 458.8, and 458.2 eV, respectively. The observed Ti^{3+} deconvolution peaks indicated the presence of oxygen vacancy caused by heat treatment and implied that O was substituted with N in a TiO_2 lattice. To examine the calcination effect on N doping further, the FTIR spectra of P-25 and TiO_xN_y were compared (Fig. 3). The sharp absorption peak near 500 cm^{-1} was assigned to the vibration level of the Ti–N bond [26,27], and NH_3 was adsorbed onto the catalyst because of the presence of N–H bending vibrations in the wave numbers of 1401 cm^{-1} and 1537 cm^{-1} [28,29].

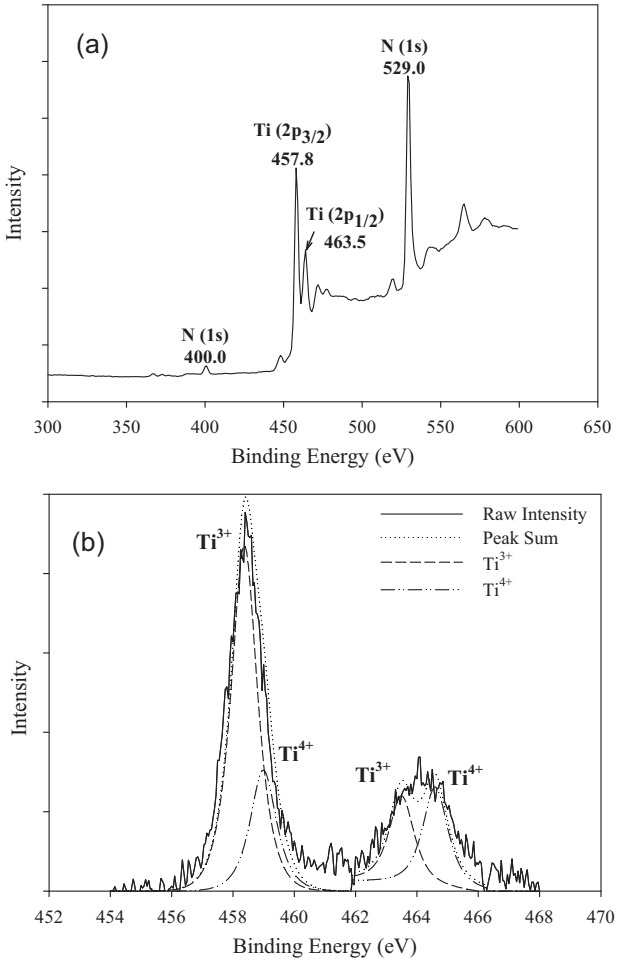

Fig. 2. (a) The survey spectrum and (b) the deconvolution of Ti 2p peaks between 454 and 468 eV for TiO_xN_y sample.

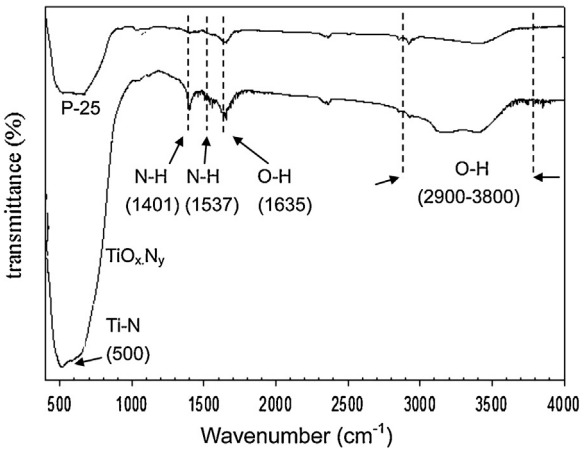

Fig. 3. FTIR spectra of raw P-25 and TiO_xN_y.

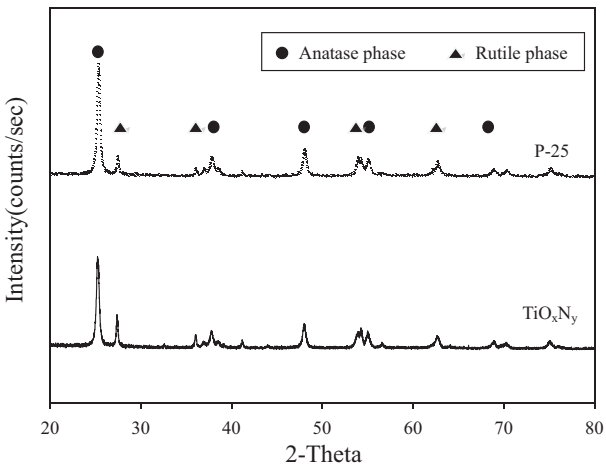

Fig. 5. XRD spectra of raw P-25 and TiO_xN_y.

Fig. 4 shows the UV/Vis diffuse reflectance spectra for as-prepared TiO_xN_y and raw P-25 TiO_2 as reference material. The absorption spectrum of the P-25 showed stronger absorption than did that of TiO_xN_y at a wavelength below 340 nm, whereas the absorption spectrum of TiO_xN_y showed more absorption than did those of P-25 in a range of 360–600 nm, indicating the existence of possible surface states, presumably the oxygen vacancy states produced from the heat treatment. According to Nakamura et al. [30], oxygen vacancy states occur in TiO_2 above the valence band, participate in a new photoexcitation process, and modify the feature of absorption spectra, which can be produced during thermal treatment. Oxygen vacancy formation can be described by the following chemical equation:

$$O_o^x \xrightarrow{TiO_2} V_O^{hh} + 2e^- + \tfrac{1}{2}O_{2(g)} \quad (4)$$

where the Kröger–Vink defect notation is used to denote the positively (2+) charged oxide ion vacancy (V_O^{hh}). This reaction is induced by heat treatment, particularly in an oxygen-lean environment during TiO_xN_y preparation. Therefore, for P-25 TiO_2, only one absorption edge appeared at the wavelength below 350 nm, whereas, for the TiO_xN_y samples, a second absorption edge in the longer wavelength side appeared because of the presence of N, which was possibly derived from the mixing of 2p states of the N with O 2p states [19,23,31]. Furthermore, the oxygen vacancies produced during thermal treatment may induce an energy shift in the bandgap because of the formation of localized energy levels within the bandgap [30].

Calcination inevitably caused phase transformation and the sintering of nanocrystallites, affecting the microstructures and properties of the TiO_xN_y particles. To investigate the calcination effect on TiO_xN_y phase transformation, XRD experiments were conducted. Fig. 5 shows the XRD spectra of P-25 and TiO_xN_y and indicates that the crystal lattice of the anatase phase decreased and the lattice of the rutile phase increased after calcination because of an elevated temperature and the addition of NH_4Cl. In addition, under a high-temperature calcination condition, the generated oxygen vacancies in the TiO_xN_y can possibly promote crystallite growth and the transformation of anatase to rutile [24,32]. The crystallite size was estimated by analyzing the TEM photographs shown in Fig. 6. The average sizes of P-25 and TiO_xN_y were 30 nm and 32.4 nm, respectively. These results indicated that the crystallite size increased as the calcination temperature increased because the rutile phase fraction increased (Fig. 5). Furthermore, the BET results indicated that the specific surface areas of P-25 and TiO_xN_y were 55 m^2/g and 48 m^2/g, respectively, supporting that agglomeration occurred because of the calcination procedure performed to reduce the specific surface area.

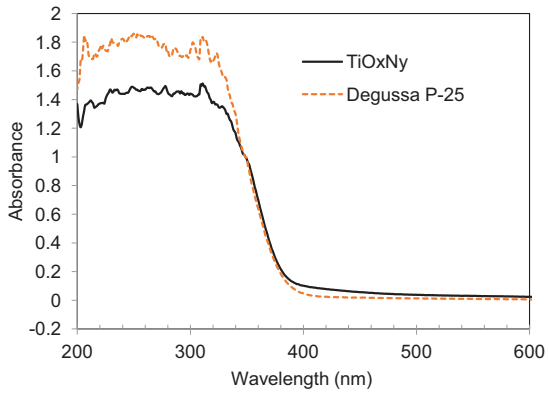

Fig. 4. UV/Vis diffuse reflectance spectra of raw P-25 and TiO_xN_y.

3.2. Hg removal by using raw P-25 and TiO_xN_y and the adsorption/desorption mechanisms

3.2.1. 25 °C experiments

Figs. 7–9 illustrate the Hg adsorption–desorption dependencies of raw P-25 and TiO_xN_y nanoparticles on various test parameters, including O_2 concentration, the presence of humidity, type of light source, and temperature. These parameters were alternately evaluated by gradually increasing the O_2 concentration from 0 to 6 and then to 21% in addition to introducing H_2O (24.5% relative humidity) and UV/VL irradiation to the photocatalytic reactor. The average Hg^0 removal efficiencies (E_{cap}) are summarized in Tables 1 and 2 for clarity. Tests were first conducted under the 0% O_2, dry (H_2O < 0.1 vol%), and dark condition. The values of E_{cap} of P-25 and TiO_xN_y at 25 °C were 1.58% and 7.67%, respectively, in Runs 0–10 (Fig. 7), indicating that most of the inlet Hg passed through the photocatalytic reactor instantly. This result was expected and similar to that of our previous study [33] because Hg^0 appeared to be the major Hg species under the test condition and exhibited difficulty in forming a strong bond with the titania surface under the dark condition. However, P-25 and TiO_xN_y exhibited substantial enhancements in E_{cap} (Runs 11–20) up to 36.6% and 19.4%, respectively, after UV irradiation was applied. These observations indicated that both samples exhibited high photocatalytic potential for transforming Hg^0 into Hg^{2+} caused by the surface-adsorbed oxygen of nanoparticles. Furthermore, these

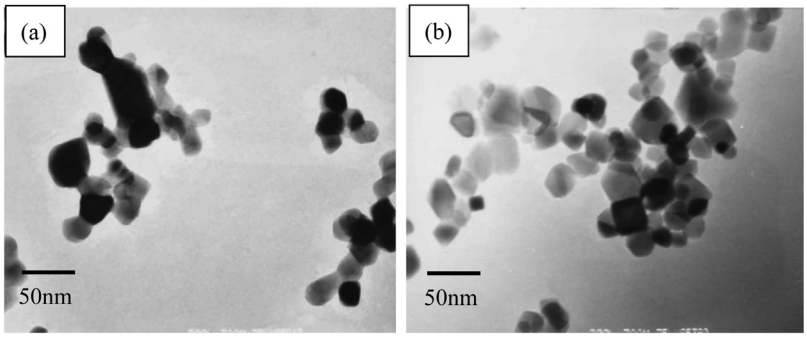

Fig. 6. TEM photographs of (a) raw P-25 and (b) TiO_xN_y.

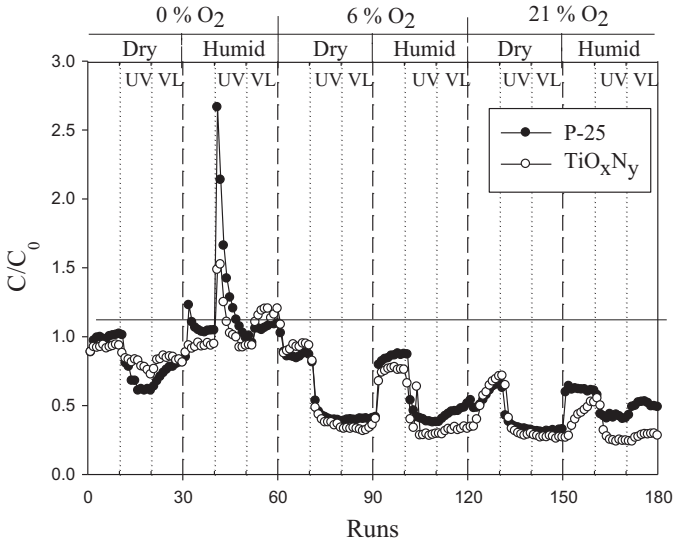

Fig. 7. Hg^0 removal dependence on the presence of light irradiation, O_2, and moisture at 25 °C.

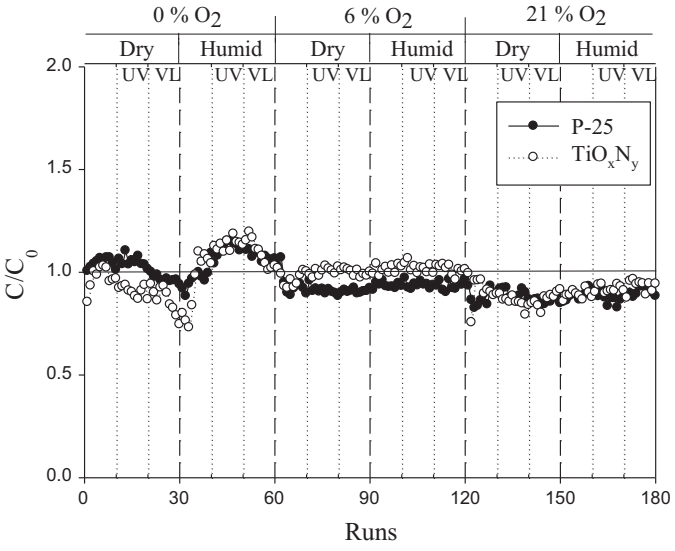

Fig. 9. Hg^0 removal dependence on the presence of light irradiation, O_2, and moisture at 100 °C.

experimental results suggested that Hg^0 primarily reacts heterogeneously in an adsorbed state on the TiO_2 surface, and does not directly react in the gas phase through homogeneous catalysis [33,34]. Two additional points must be mentioned. First, VL irradiation exhibited less effectiveness in inducing the transformation of Hg^0 into Hg^{2+} under the 0% O_2 dry condition than UV irradiation did regardless of which nanoparticles were used. Second, raw P-25 yielded a greater E_{cap} than TiO_xN_y did under the 0%

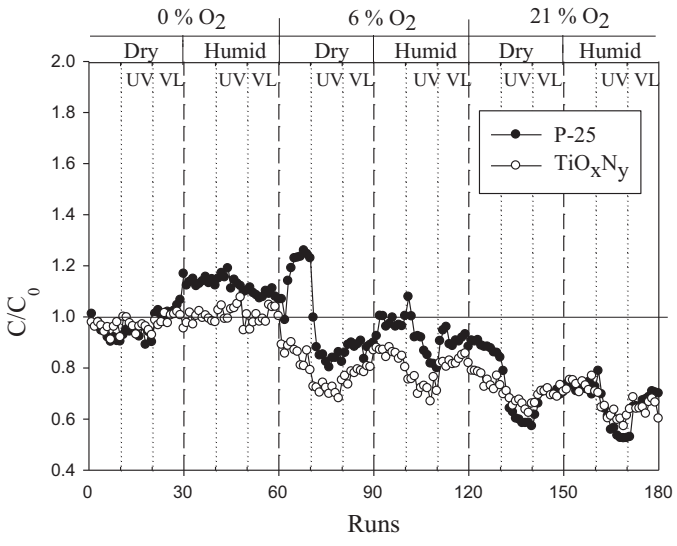

Fig. 8. Hg^0 removal dependence on the presence of light irradiation, O_2, and moisture at 50 °C.

Table 1
Average Hg removal efficiency (E_{cap} in %; mean ± standard deviation) for raw P-25 nanoparticles under various experimental conditions (n = 10).

		Dark	UV	VL
25 °C	0% O_2-dry	1.58 ± 3.57	36.6 ± 15.8	35.0 ± 7.55
	6% O_2-dry	12.0 ± 5.00	53.8 ± 12.4	60.1 ± 0.55
	21% O_2-dry	43.2 ± 6.58	62.2 ± 8.81	68.7 ± 0.69
	0% O_2-humid	−3.21 ± 12.8	−45.8 ± 52.1	−5.33 ± 4.13
	6% O_2-humid	19.6 ± 13.2	53.9 ± 14.4	55.1 ± 3.75
	21% O_2-humid	41.4 ± 8.75	54.5 ± 6.93	51.0 ± 3.89
50 °C	0% O_2-dry	1.00 ± 3.54	−3.07 ± 5.78	−19.3 ± 2.02
	6% O_2-dry	−23.1 ± 8.50	9.36 ± 5.11	6.71 ± 2.03
	21% O_2-dry	6.96 ± 2.13	32.3 ± 6.39	25.9 ± 2.93
	0% O_2-humid	−18.5 ± 1.18	−18.6 ± 2.88	−13.9 ± 1.49
	6% O_2-humid	−2.52 ± 2.43	5.14 ± 8.43	3.72 ± 2.44
	21% O_2-humid	22.5 ± 1.35	35.3 ± 8.40	28.8 ± 4.94
100 °C	0% O_2-dry	−1.47 ± 2.20	−2.18 ± 2.36	6.05 ± 1.61
	6% O_2-dry	8.86 ± 4.82	12.08 ± 1.04	11.64 ± 0.82
	21% O_2-dry	14.8 ± 3.36	13.8 ± 2.52	16.6 ± 1.41
	0% O_2-humid	5.59 ± 5.10	−8.39 ± 3.22	−4.08 ± 2.27
	6% O_2-humid	8.58 ± 1.48	9.17 ± 1.08	9.08 ± 2.06
	21% O_2-humid	13.1 ± 2.09	15.2 ± 2.51	11.9 ± 1.74

Table 2
Average Hg removal efficiency (E_{cap} in %; mean ± standard deviation) for TiO_xN_y nanoparticles under various experimental conditions (n = 10).

		Dark	UV	VL
25 °C	0% O_2-dry	7.67 ± 1.44	19.4 ± 4.33	16.9 ± 2.66
	6% O_2-dry	6.15 ± 5.36	56.7 ± 13.6	66.8 ± 1.12
	21% O_2-dry	41.6 ± 12.5	65.6 ± 10.7	72.9 ± 0.58
	0% O_2-humid	7.05 ± 1.96	−11.6 ± 21.5	−12.1 ± 9.75
	6% O_2-humid	28.5 ± 10.8	62.5 ± 14.1	67.4 ± 1.57
	21% O_2-humid	55.4 ± 8.06	72.0 ± 7.62	72.1 ± 1.63
50 °C	0% O_2-dry	5.21 ± 3.85	3.76 ± 2.42	1.12 ± 2.65
	6% O_2-dry	12.5 ± 5.18	27.9 ± 2.89	22.1 ± 2.14
	21% O_2-dry	23.5 ± 3.13	32.7 ± 3.13	30.4 ± 2.18
	0% O_2-humid	0.86 ± 2.01	−1.67 ± 3.65	−0.19 ± 3.01
	6% O_2-humid	13.6 ± 1.46	26.2 ± 3.65	18.5 ± 3.85
	21% O_2-humid	26.8 ± 2.10	36.8 ± 4.27	35.1 ± 2.27
100 °C	0% O_2-dry	2.57 ± 5.04	9.29 ± 2.49	13.3 ± 6.22
	6% O_2-dry	3.30 ± 3.15	−0.61 ± 1.75	0.27 ± 1.50
	21% O_2-dry	9.70 ± 5.67	14.9 ± 2.29	13.1 ± 3.15
	0% O_2-humid	5.38 ± 13.8	−13.3 ± 2.48	−9.23 ± 6.27
	6% O_2-humid	−1.92 ± 2.11	−2.08 ± 2.14	−0.97 ± 2.22
	21% O_2-humid	10.5 ± 1.67	8.33 ± 2.07	6.19 ± 2.12

O_2 dry condition, possibly because the amount of rutile phase for TiO_xN_y was greater than that for raw P-25 and the larger particle size and smaller surface area of TiO_xN_y caused it to absorb less O_2. In addition, Lee et al. [7] suggested that anatase is more effective in oxidizing Hg^0 than rutile. Consequently, the physical properties of TiO_2 can influence Hg^0 transformation under the 0% O_2 dry condition.

Moisture caused desorption of Hg species from the TiO_2 surface, particularly after UV irradiation was applied (Runs 41–50; E_{cap} = −45.8% and −11.6% for P-25 and TiO_xN_y, respectively; Fig. 7 and Tables 1 and 2). The competitive adsorption of H_2O and reemission of adsorbed Hg species into the gas phase caused by the alteration of the surface properties of TiO_2 by light irradiation were thus validated [9,10,33,35,36]. Previous studies have suggested that enhancement in the surface hydrophilicity of TiO_2 may occur because of light irradiation [33,37]. This enhancement may not influence the photocatalytic ability of TiO_2 or Hg removal of TiO_2; however, the enhancement may increase the affinity of a TiO_2 surface to H_2O, thereby causing the reemission of Hg.

Overall, TiO_xN_y exhibited high resistance against the competition of H_2O on the adsorption sites of TiO_2 (Fig. 7). The total Hg desorption percentage (i.e., the integrated area for C/C_o >1 divided by that for C/C_o <1) between Runs 30 and 60 was approximately 12% of the total Hg adsorption of TiO_xN_y. By contrast, the Hg desorption of P-25 was approximately 50% of the total Hg adsorption. These experimental results suggested that certain functionality introduced during the NH_4Cl thermal treatment may form strong bonding with the adsorbed Hg species [38]. The N–H and –O–H groups may form chemical bonds with Hg^0 or with oxidized Hg (e.g., HgO). Thus, competition for these chemical functional groups from H_2O may be less pronounced compared to that for the inherent functionality in raw P-25. VL irradiation caused increased desorption of Hg from TiO_xN_y under the 0% O_2 humid condition (E_{cap} = −12.1%), indicating that NH_4Cl treatment increased the surface hydrophilicity of TiO_xN_y when it was irradiated with VL.

Increasing the O_2 concentration generally enhanced the Hg^0 removal of both P-25 and TiO_xN_y nanoparticles (Runs 61–240; Fig. 7 and Tables 1 and 2). This enhancement was primarily caused by the increasing catalytic oxidation of Hg^0. In addition, these experimental results are consistent with those of our previous studies on oxygen-vacant TiO_{2-x} [33,35]. Even under the dark condition, both P-25 and TiO_xN_y exhibited substantial Hg^0 removal of up to 55.4% when the O_2 content was 21%. These test results confirmed that TiO_2 exhibits prominent catalytic and adsorption properties in the presence of O_2, even when it is not irradiated by light. After TiO_xN_y was excited by UV light, the E_{cap} increased to approximately 62.5% when the O_2 concentration was 6% and to approximately 72.0% when the O_2 concentration was 21% (humid condition), indicating that light irradiation, particularly UV irradiation, further increased Hg oxidation and removal. These results verified that the catalytic oxidation of Hg^0 into Hg^{2+} under an oxygen-rich condition, in association with the subsequent adsorption of oxidizing Hg species, caused the enhancement in Hg removal by TiO_2 nanoparticles [33,35]. In the presence of O_2, TiO_xN_y generally exhibited greater Hg removal than did raw P-25, particularly under the humid condition (i.e., during Runs 91–120 and Runs 151–180; Fig. 7). These results suggested that TiO_xN_y is more resistant to H_2O competition in the presence of O_2 than P-25. O_2 may either form a stronger bond with TiO_xN_y (i.e., surface chemisorbed O) or enhance heterogeneous catalysis, causing additional chemical bonds between Hg and O–H and N–H groups to form. Both phenomena appeared to reduce the competition from H_2O molecules for adsorption sites.

Two results observed in our previous study [33] were also observed in this study. First, the E_{cap} of both TiO_2 samples observed under the humid condition was typically smaller when VL rather than UV light was the irradiation source. Second, when UV light was the irradiation source, the differences in E_{cap}, particularly in that of TiO_xN_y, observed in the dry and humid tests were minor when the O_2 concentration was > 6%. These observations implied that when UV was the irradiation source, the H_2O adsorbed on the TiO_2 surface may successfully form OH· radicals, enhancing the catalytic oxidation of Hg^0. Consequently, the humidity slightly affected E_{cap} when UV irradiation was applied. This mechanism was evident when TiO_xN_y was tested. In addition, because TiO_xN_y is a VL-type photocatalyst, the differences in the E_{cap} observed in the dry and humid tests performed using VL irradiation were minor (Table 2) because the adsorbed H_2O could be transformed into $OH^•$ radicals. By contrast, particularly when VL irradiation was applied to the raw P-25, the transformation of adsorbed H_2O into $OH^•$ radicals was less effective. H_2O molecules bound to the hydrophilic surface of raw P-25 occupied the oxidation and adsorption sites for Hg species, causing the E_{cap} to be lower than that during UV irradiation. The minor activity of the VL-type TiO_2 photocatalyst during VL irradiation may also be affected by particle size, crystal phase, UV/Vis light absorption spectra, and the doping status [39]. In addition, the photocatalytic reduction of HgO to Hg^0 induced by free electrons generated on the TiO_2 surface during UV irradiation may have occurred when VL was applied to the raw P-25, increasing reemission of adsorbed Hg [9].

3.2.2. 50 and 100 °C experiments

Generally, Hg removal tested at elevated temperatures exhibited similar dependence on the presence of UV and VL light, O_2, and moisture at 25 °C (Figs. 8 and 9; Tables 1 and 2). However, elevating the temperature to 50 °C and 100 °C substantially reduced the Hg removal of both raw P-25 and TiO_xN_y, suggesting that the adsorption of Hg species was thermally unfavorable because of the exothermic behavior of adsorption. TiO_xN_y exhibited superior performance in Hg adsorption compared with raw P-25 and underwent little adsorption competition from H_2O at high temperatures. These results suggested that the N–H and –O–H groups may form strong chemical bonds with Hg at high temperature. O_2 at 21% remained a suitable enhancer in Hg oxidation/adsorption at 50 °C and 100 °C; nevertheless, the adsorption capacity was not comparable to that observed at 25 °C. At 100 °C, the adsorption performance of raw P-25 and TiO_xN_y was low, and the E_{cap} was only between 6.19% and 16.6% when the O_2 concentration was 21% (Tables 1 and 2).

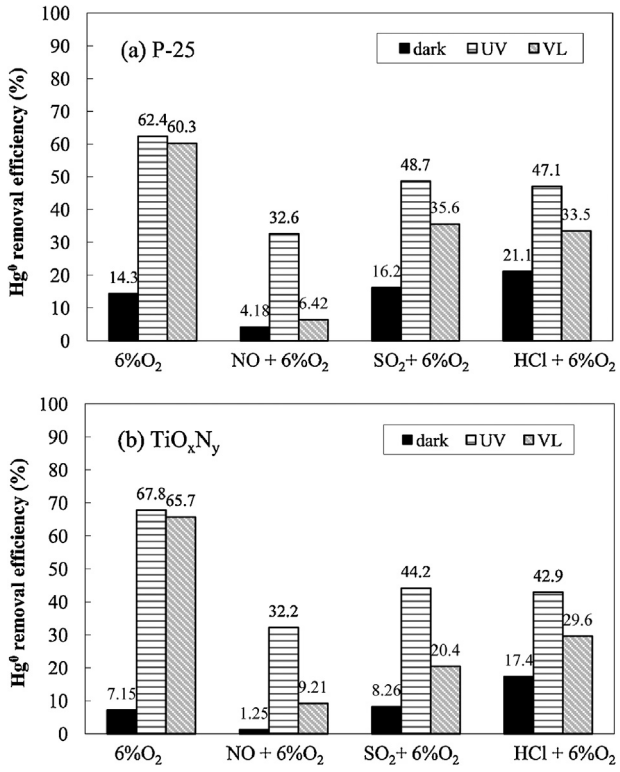

Fig. 10. Average Hg^0 removal of raw P-25 and TiO_xN_y with the presence of acidic gas components.

3.2.3. Effects of NO, SO_2, and HCl on Hg^0 removal

The effects of NO (200 ppm_v), SO_2 (200 ppm_v), and HCl (50 ppm_v) on the Hg^0 removal of TiO_2 samples were tested when the O_2 concentration was 6%, the temperature was 25 °C, and the relative humidity was 24.5%. The flue gas components individually flow into the reaction chamber, and thus, the potential interactions between these acidic components were neglected. Generally, the presence of NO markedly reduced E_{cap} under various light irradiations (Fig. 10), indicating that the NO molecules may compete with the adsorption sites on the TiO_2 surface. In addition, Yuan et al. [40] suggested that NO competes with O_2^- and •OH free radicals to form NO_2, reducing the transformation of Hg^0 into HgO and, thus, reducing Hg adsorption. By contrast, two scenarios were observed when SO_2 and HCl were introduced. Under the dark condition, both SO_2 and HCl slightly enhanced the Hg adsorption. In addition, raw P-25 and TiO_xN_y exhibited substantial increases from 14.3% to 21.1% and from 7.15% to 17.4%, respectively, when HCl was introduced (Fig. 10). These results indicated that both SO_2 and HCl can enhance Hg^0 oxidation and subsequent Hg adsorption even without light irradiation. By contrast, under both UV and VL irradiation, the presence of SO_2 or HCl significantly decreased the E_{cap}, from 60.3–67.8% to 20.4–48.7%. We suspect that both SO_2 and HCl may consume a substantial number of O_2^- and ·OH free radicals during light irradiation, similar to the role that NO plays, and subsequently reduce the transformation of Hg^0 into HgO. In addition, SO_2 may have reacted with O_2 to catalytically form SO_3 when light irradiation was applied. The formed SO_3, instead of forming $HgSO_4$ captured by TiO_2 as suggested by Yuan et al. [40] and Li et al. [41], may have adhered to the adsorbent surface and occupied the original adsorption sites for Hg species. Consequently, the E_{cap} decreased accordingly in the presence of SO_2 and light irradiation.

4. Conclusion

N-doped TiO_2 nanoparticles exhibiting a narrow bandgap were prepared by calcinating a mixture of Degussa P-25 TiO_2 and NH_4Cl at a temperature of 400 °C under airtight conditions to remove gaseous Hg^0. XPS and UV/Vis diffuse reflectance spectra indicated that the molecular state N was incorporated into a TiO_2 lattice, causing an observable shift of the absorption edge to a long wavelength of 441 nm. The formed nanoparticles exhibited a size of 32.4 nm and were in a mixed form of anatase and rutile according to the XRD spectra. The minor Hg removal of both raw P-25 and TiO_xN_y under O_2-lean and dark conditions suggested that the photocatalytic oxidation of Hg^0 transformation into Hg^{2+} (i.e., HgO) is a key step in enhancing Hg adsorption. Both physical (e.g., particle size, surface area, and crystalline phase of TiO_2) and chemical properties (e.g., surface functionality) can influence Hg^0 transformation and adsorption as well as the resistance to competition on adsorption sites from H_2O. The enhancement of the surface hydrophilicity of TiO_2, which caused the reemission of adsorbed Hg species, can be substantially inhibited by N modification. In addition, TiO_xN_y acts as a VL-type photocatalyst. The difference in average Hg removal observed in the dry and humid tests during visible-light irradiation at >6% O_2 was minor, and TiO_xN_y underwent little adsorption competition from H_2O at high temperatures. The flue gas components (NO, SO_2, and HCl) produced diverse effects, generally causing a reduction in Hg adsorption when light irradiation was applied. The obtained data suggested that the bonding between TiO_xN_y and Hg species is loose and that the adsorption and desorption processes seem to be easily reversed. Applying advanced surface modification on TiO_2 nanoparticles to resist the competitive adsorption from moisture and negative photocatalytic effects produced by flue gas components is the key to successfully applying this technique in pilot tests and full-scale application.

Acknowledgements

This work was financially supported by Ministry of Science and Technology, Taiwan (100-2211-E-002-256-MY3). The authors also acknowledge Dr. Chia-Hung Huang, Industrial Technology Research Institute (ITRI), Taiwan for his technical assistance in light intensity measurements.

References

[1] E.G. Pacyna, J.M. Pacyna, K. Sundseth, J. Munthe, K. Kindbom, S. Wilson, F. Steenhuisen, P. Maxson, Atmos. Environ. 44 (2010) 2487–2499.
[2] UNEP News Centre website, Minamata Convention Agreed by Nations, http://www.unep.org/newscentre/default.aspx?DocumentID=2702&ArticleID=9373&l=en, 2013.
[3] H.-C. Hsi, H.-H. Lee, J.-F. Hwang, W. Chen, J. Air Waste Manage Assoc. 60 (2010) 514–522.
[4] E. Pitoniak, C.-Y. Wu, D. Londeree, D. Mazyck, J.-C. Bonzongo, K. Powers, W. Sigmund, J. Nanopart. Res. 5 (2003) 281–292.
[5] E. Pitoniak, C.-Y. Wu, D.W. Mazyck, K.W. Powers, W. Sigmund, Environ. Sci. Technol. 39 (2005) 1269–1274.
[6] C.-Y. Wu, T.G. Lee, G. Tyree, E. Arar, P. Biswas, Environ. Eng. Sci. 15 (1998) 137–148.
[7] T.G. Lee, P. Biswas, E. Hedrick, Ind. Eng. Chem. Res. 43 (2004) 1411–1417.
[8] A. Suriyawong, M. Smallwood, Y. Li, Y. Zhuang, P. Biswas, Aerosol Sci. Technol. 9 (2009) 394–403.
[9] Y. Li, C.-Y. Wu, Environ. Sci. Technol. 40 (2006) 6444–6448.
[10] Y. Li, C.-Y. Wu, Environ. Eng. Sci. 24 (2007) 3–12.
[11] Y. Li, P.D. Murphy, C.-Y. Wu, K.W. Powers, J.-C.J. Bonzongo, Environ. Sci. Technol. 42 (2008) 5304–5309.
[12] H. Wang, S. Zhou, L. Xiao, Y. Wang, Y. Liu, Z. Wu, Catal. Today 175 (2011) 202–208.
[13] S.U.M. Khan, M. Al-Shahry, W.B. Ingler, Science 297 (2002) 2243–2245.
[14] R. Asahi, T. Morikawa, T. Ohwaki, K. Aoki, Y. Taga, Science 293 (2001) 269–271.
[15] T. Morikawa, R. Asahi, T. Ohwaki, K. Aoki, Y. Taga, Jpn. J. Appl. Phys., Part 2 40 (2001) L561–L563.
[16] T. Umebayashi, T. Yamaki, H. Itoh, K. Asai, Appl. Phys. Lett. 81 (2002) 454–456.
[17] S. Sato, Chem. Phys. Lett. 123 (1986) 126–128.

[18] K. Kobayakawa, Y. Murakami, Y. Sato, J. Photochem. Photobiol. A 170 (2005) 177–179.
[19] S. Livraghi, A. Votta, M.C. Paganini, E. Giamello, in: C.C. Aldo Gamba, C. Salvatore (Eds.), Stud. Surf. Sci. Catal., Elsevier, 2005, pp. 375–380.
[20] N. Martin, O. Banakh, A.M.E. Santo, S. Springer, R. Sanjinés, J. Takadoum, F. Lévy, Appl. Surf. Sci. 185 (2001) 123–133.
[21] Y. Nosaka, M. Matsushita, J. Nishino, A.Y. Nosaka, Sci. Technol. Adv. Mat. 6 (2005) 143–148.
[22] H. Irie, Y. Watanabe, K. Hashimoto, J. Phys. Chem. B 107 (2003) 5483–5486.
[23] B. Kosowska, S. Mozia, A.W. Morawski, B. Grzmil, M. Janus, K. Kałucki, Solar Energy Mater. Solar Cells 88 (2005) 269–280.
[24] B.C. Hsu, S.S. Chen, C. Su, Y.T. Liu, J. Nanosci. Nanotechno. 7 (2007) 3104–3110.
[25] O. Diwald, T.L. Thompson, T. Zubkov, S.D. Walck, J.T. Yates, J. Phys. Chem. B 108 (2004) 6004–6008.
[26] L.I. Wei, J.-F. Chen, Appl. Surf. Sci. 253 (2007) 7019–7023.
[27] N. Saoula, K. Henda, R. Kesri, J. Plasma Fusion Res. 8 (2009) 1403–1407.
[28] Y. Zhao, X. Qiu, C. Burda, Chem. Mater. 20 (2008) 2629–2636.
[29] X.-Z. Bu, G.-K. Zhang, Y.-Y. Gao, Y.-Q. Yang, Microporous Mesoporous Mater. 136 (2010) 132–137.
[30] I. Nakamura, N. Negishi, S. Kutsuna, T. Ihara, S. Sugihara, K. Takeuchi, J. Mol. Catal. A: Chem. 161 (2000) 205–212.
[31] R. Nakamura, T. Tanaka, Y. Nakato, J. Phys. Chem. B 108 (2004) 10617–10620.
[32] T. Bak, J. Nowotny, M.K. Nowotny, J. Phys. Chem. B 110 (2006) 21560–21567.
[33] H.-C. Hsi, C.-Y. Tsai, Chem. Eng. J. 191 (2012) 378–385.
[34] A.A. Presto, E.J. Granite, Environ. Sci. Technol. 40 (2006) 5601–5609.
[35] C.-Y. Tsai, H.-C. Hsi, H. Bai, K.-S. Fan, C. Chen, J. Nanopart. Res. 13 (2011) 4739–4748.
[36] Y. Li, P. Murphy, C.-Y. Wu, Fuel Process. Technol. 89 (2008) 567–573.
[37] A. Fujishima, T.N. Rao, D.A. Tryk, J. Photochem. Photobiol. C 1 (2000) 1–21.
[38] Z. Tan, L. Sun, J. Xiang, H. Zeng, Z. Liu, S. Hu, J. Qiu, Carbon 50 (2012) 362–371.
[39] C. Chen, H. Bai, C. Chang, J. Phys. Chem. C 111 (2007) 15228–15235.
[40] Y. Yuan, J. Zhang, H. Li, Y. Li, Y. Zhao, C. Zheng, Chem. Eng. J. 192 (2012) 21–28.
[41] H. Li, C.-Y. Wu, Y. Li, J. Zhang, Environ. Sci. Technol. 45 (2011) 7394–7400.